

Asymmetric Catalysis Upon Helically Chiral Loratadine Analogs Unveils Enantiomer-Dependent Antihistamine Activity

Elizabeth A Stone, Kara J Cutrona, and Scott J. Miller

J. Am. Chem. Soc., **Just Accepted Manuscript** • DOI: 10.1021/jacs.0c03904 • Publication Date (Web): 24 Jun 2020

Downloaded from pubs.acs.org on June 24, 2020

Just Accepted

“Just Accepted” manuscripts have been peer-reviewed and accepted for publication. They are posted online prior to technical editing, formatting for publication and author proofing. The American Chemical Society provides “Just Accepted” as a service to the research community to expedite the dissemination of scientific material as soon as possible after acceptance. “Just Accepted” manuscripts appear in full in PDF format accompanied by an HTML abstract. “Just Accepted” manuscripts have been fully peer reviewed, but should not be considered the official version of record. They are citable by the Digital Object Identifier (DOI®). “Just Accepted” is an optional service offered to authors. Therefore, the “Just Accepted” Web site may not include all articles that will be published in the journal. After a manuscript is technically edited and formatted, it will be removed from the “Just Accepted” Web site and published as an ASAP article. Note that technical editing may introduce minor changes to the manuscript text and/or graphics which could affect content, and all legal disclaimers and ethical guidelines that apply to the journal pertain. ACS cannot be held responsible for errors or consequences arising from the use of information contained in these “Just Accepted” manuscripts.

Asymmetric Catalysis Upon Helically Chiral Loratadine Analogs Unveils Enantiomer-Dependent Antihistamine Activity

Elizabeth A. Stone, Kara J. Cutrona, and Scott J. Miller*

Department of Chemistry, Yale University, P. O. Box 208107, New Haven, Connecticut 06520-8107, United States

KEYWORDS: loratadine • *N*-oxidation • peptide-catalysis • helical-chirality • antihistamine

ABSTRACT: Analogs of the conformationally dynamic Claritin® (loratadine) and Clarinex® (desloratadine) scaffolds have been enantio- and chemoselectively *N*-oxidized using an aspartic acid containing peptide catalyst to afford stable, helically chiral products in up to >99:1 er. The conformational dynamics and enantiomeric stability of the *N*-oxide products have been investigated experimentally and computationally with the aid of crystallographic data. Furthermore, biological assays show that rigidifying the core structure of loratadine and related analogs through *N*-oxidation affects antihistamine activity in an enantiomer-dependent fashion. Computational docking studies illustrate the observed activity differences.

Introduction

Since its discovery in the 1980s, Claritin® (loratadine, **1a**) has been effective, invaluable, and ubiquitous as an antihistamine. While initially used to treat allergies,¹ loratadine (**1a**) and related analogs (**2–3**; Figure 1a) have exhibited additional biological activity against cancer,² melanogenesis,³ biofilms,⁴ antibiotic resistance,⁴ as well as mood and metabolic disorders.⁵ This diverse biological activity may be linked to the intriguing conformational topology of **1a**. For example, loratadine (**1a**) and desloratadine (**2**), an even more potent antihistamine,⁶ are conformationally dynamic, interconverting rapidly at room temperature between enantiomeric, helically chiral forms.

More generally, conformationally dynamic drugs and drug candidates that exhibit enantiomeric, interconverting ground states are a topic of intense current interest, most commonly in consideration of various forms of atropisomerism.⁷ While the conformational dynamics in the loratadine scaffold have attracted some attention,⁸ the differential biological activity of small molecules exhibiting helical chirality, devoid of any point-chiral element or an axis of chirality, has received much less attention. Accordingly, the molecular basis of conformation-specific binding of loratadine-like enantiomers is not well understood.

In a study related to lonafarnib (**3**), Morgan *et al.* noted that bromination of the arene (green bromine, Figure 1b) gave rise to the chiral, racemic product (\pm)-**4**.^{8c} Using a lipase, a kinetic resolution (KR) of racemic **4** was performed to afford enantioenriched (+)-**5**, which was then elaborated synthetically into **3**, a compound whose stereochemistry stems primarily from its point-chirality. In related scaffolds, we sought an alternative, more efficient strategy for establishing and studying this

relatively unique form of helical chirality through asymmetric catalysis. Recently, we reported the enantioselective *N*-oxidation of substituted (bis)pyridines using an aspartic acid embedded peptide catalyst (Figure 1c).⁹ We anticipated that this method could be applied to the synthesis of a loratadine analog (**6a**) exhibiting helical chirality induced *via* pyridine *N*-oxidation (Figure 1d). Notably, loratadine *N*-oxide (**6a**) itself was described as a metabolite of loratadine¹⁰ and has been synthesized as a platform to access derivatives of **1a**.¹¹ However, to the best of our knowledge, **6a** has not been synthesized enantioselectively, nor have the structural and medicinal properties of the individual enantiomers (+)-**6a** and (–)-**6a** been studied.

Our approach relies on the dynamic kinetic resolution (DKR) of loratadine analogs (**1a**) to afford an enantiomerically enriched *N*-oxide product (**6a**) in a single step, an advance from the existing strategy to access helically chiral loratadine analogs that relies on non-selective bromination followed by KR of the racemic bromoarene (Figure 1d).^{2a, 8c} Herein, we extend upon the first report of a catalytic, asymmetric synthesis of pyridine *N*-oxide derivatives employing aspartic acid containing peptides.⁹ Of particular note, our previous study included a singular example of this type of transformation on a loratadine-like skeleton, albeit with a substrate lacking biologically validated substituents. In this report, we demonstrate for the first time (a) the synthesis of 13 optically enriched (up to >99:1 er) loratadine *N*-oxide analogs using an even more enantioselective peptide catalyst than previously disclosed, (b) enhanced physical organic analysis of the determinants of enantioselectivity, (c) experimental and computational studies of the conformational dynamics and enantiomeric stability of the *N*-oxidized compounds, (d) a first-of-its-kind biological

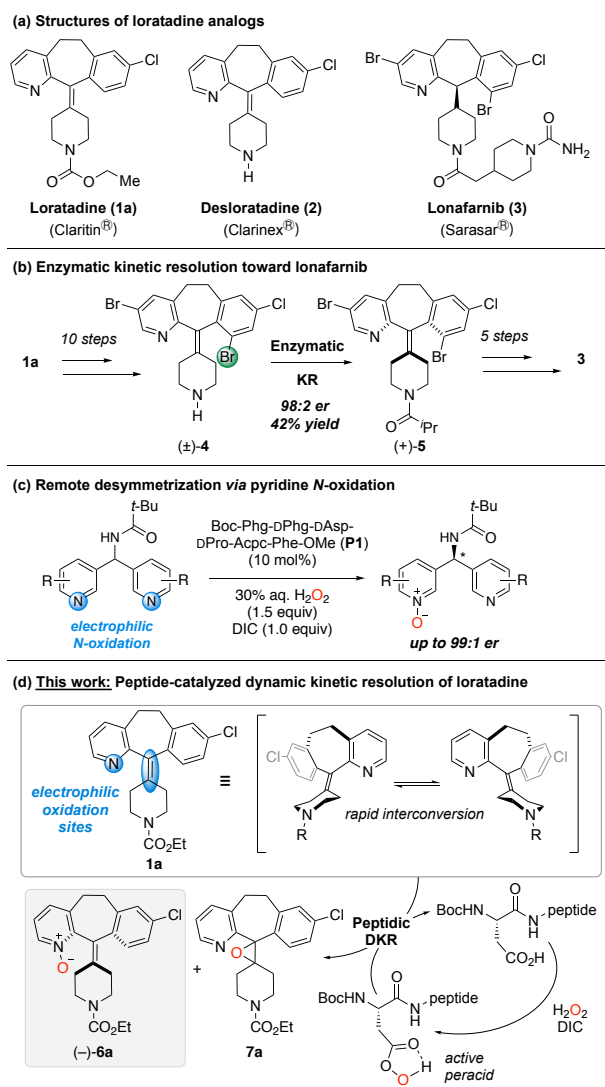


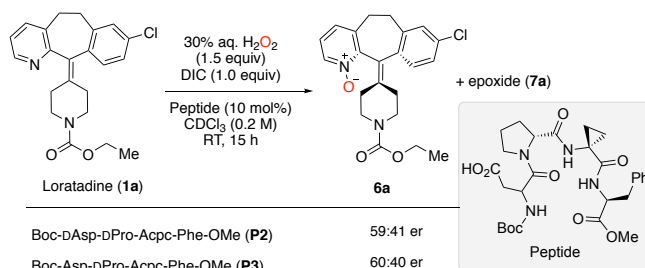
Figure 1. (a) Structures of loratadine and related analogs. (b) Enzymatic kinetic resolution (KR) of (\pm)-**4** toward lonafarnib (**3**). (c) Peptide catalyzed *N*-oxidation of bis(pyridines). (d) Peptide-catalyzed DKR of loratadine to afford helically chiral **6a**.

evaluation of the isolated loratadine *N*-oxide enantiomers (+)-**6a** and (-)-**6a**, revealing differential antihistamine activity, and (e) docking studies with the human histamine receptor that support and illuminate our experimental observations.

Results and Discussion

Synthetic Chemistry. One challenge to developing a method for selective *N*-oxidation of loratadine (**1a**) is competitive oxidation pathways, as two sites for electrophilic oxidation are present, leading to either *N*-oxidation of the pyridine (**6a**) or epoxidation (**7a**) of the neighboring olefin (Figure 1d). Previously, we have identified peptides with sequence dependent reactivity that can selectively catalyze either alkene epoxidation or Baeyer–Villiger (BV) oxidation in substrates containing both an olefin and ketone.¹² However, unlike our previous

Scheme 1. Preliminary Asp-containing peptide catalyzed oxidation of **1a**.



system, in which the catalysts were designed to distinguish between a nucleophilic olefin and electrophilic ketone, our current regime (Figure 1d) requires differentiation between functional groups of the same reactivity profile (nucleophilic), a decidedly more difficult undertaking. With this in mind, we began to explore aspartic acid containing catalysts for the enantio- and chemoselective *N*-oxidation of loratadine (**1a**, Scheme 1). After evaluating a variety of canonical β -turn inducing sequences,¹³ tetrapeptides **P2** and **P3** were identified as promising catalysts for the enantioselective *N*-oxidation of **1a** (Scheme 1).

Selectivity in many catalytic reactions may be improved by installing complementary functional groups to direct noncovalent interactions between the catalyst and substrate.¹⁴ To determine whether incorporation of an additional hydrogen bond (H-bond) donor in the starting material would improve selectivity, we continued our optimization with *N*-phenylurea substrate **1b** (Table 1), which is easily prepared from desloratadine (**2**) in a single step (see Supporting Information for details). We began by performing a series of control reactions (entries

Table 1. Reaction optimization.

30% aq. H₂O₂ (1.5 equiv), DIC (1.0 equiv)

Peptide (10 mol%), CDCl₃ (0.2 M), RT, 15 h

1b \rightarrow (-)-**6b** + **7b**

Entry	Peptide	Conv. [%] ^[a]	6b/7b ^[a]	er, 6b
1	— (<i>m</i> -CPBA) ^[b]	69	3.9:1	—
2	—	0	—	—
3	Boc-Asp-OMe	52	3.3:1	46:54
4 ^[c]	Boc-Asp-OMe	0	—	—
5	Boc-DAsp-DPro-Acpc-Phe-OMe (P2)	86	1.5:1	83:17
6	Boc-Asp-DPro-Acpc-Phe-OMe (P3)	67	5.1:1	61:39
7	Boc-DPhg-DAsp-DPro-Acpc-Phe-OMe (P1)	88	1.3:1	76:24
8 ^[d]	Boc-DAsp-DPro-Acpc-Phe-OMe (P2)	83	1.7:1	87:13
9 ^[d]	Ts-DAsp-DPro-Acpc-Phe-OMe (P4)	85	1.3:1	89:11
10 ^[d,e]	Boc-Asp(“Me)Pro-Acpc-DPhe-OMe (P5)	92	1.3:1	7:93
11 ^[d,f]	Boc-Asp(“Me)Pro-Acpc-DPhe-OMe (P5)	79	1.2:1	7:93
12 ^[d]	Ts-Asp(“Me)Pro-Acpc-DPhe-OMe (P6)	84	1.1:1	7:93

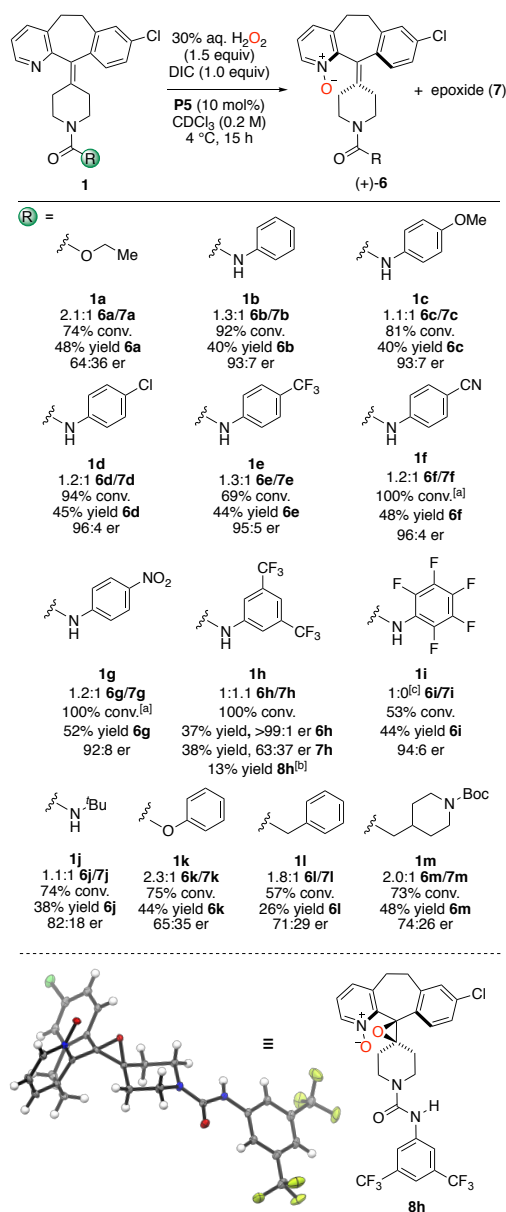
[a] All reactions were conducted in duplicate on a 0.03 mmol scale. Conversion of **1b** to **6b** + **7b** and **6b/7b** ratios were determined using ¹H NMR (CDCl₃). [b] *m*-CPBA (1.0 equiv) was used instead of H₂O₂ and DIC. [c] DIC was excluded. [d] Reaction performed at 4 °C. [e] The same results were obtained using CHCl₃ and CDCl₃. [f] Conducted in CHCl₃ using 1.0 equiv H₂O₂.

1–4, Table 1). Using 1 equiv of *m*-CPBA, 69% conversion to oxidized products (–)-**6b** and **7b** was obtained, favoring *N*-oxidation over epoxidation in a 3.9:1 ratio (entry 1). When 30% aqueous hydrogen peroxide (H₂O₂) was used as the oxidant with DIC, no reaction was observed, demonstrating the critical role of the Asp residue for catalysis (entry 2; see also Figure 1d). Addition of catalytic Boc-Asp-OMe afforded 52% conversion, favoring the *N*-oxide in a 3.3:1 ratio with detectable enantioselectivity (46:54 er; entry 3). Reactivity was ablated when DIC was excluded, reinforcing the importance of this reagent for catalyst activation (entry 4).

We then returned to assess the activity of tetrapeptides **P2** and **P3** with **1b**. Enantioselectivity improved with **P2** to 83:17 er, yet with diminished chemoselectivity (1.5:1 (–)-**6b**:**7b**) as compared to the Asp-monomer or *m*-CPBA (compare entry 5 to entries 1 and 3, respectively). Conversely, **P3**, bearing L- instead of D-Asp, was less enantioselective (61:39 er), but significantly favored *N*-oxidation over epoxidation in a 5.1:1 ratio (entry 6). Having achieved excellent chemoselectivity with **P3**, we sought to improve the enantioselectivity of the *N*-oxidized material. In our previously reported *N*-oxidation of bis(pyridines) (Figure 1c),⁹ **P1** was identified as the lead catalyst; however, **P2** proved to be superior in both chemo- and enantioselectivity with **1b** (entry 5 vs. 7). Lowering the temperature to 4 °C with **P2** was found to be optimal for balancing conversion (83%) with enantio- (87:13 er) and chemoselectivity (1.7:1 ratio; entry 8). We then examined the *N*-terminal protecting group of the peptide and found that incorporation of an electron withdrawing tosyl group (**P4**) provided 85% conversion and further enhanced enantioinduction (89:11 er) with a 1.3:1 ratio of **6b**/**7b** (entry 9). Additionally, **P5** containing a methyl group at the α -position of the proline residue (α -Me(Pro)) was synthesized, as it was hypothesized to block one face of the peptide catalyst, curbing unselective substrate-catalyst binding. Indeed, **P5** achieved 92% conversion to a 1.3:1 ratio of **6b**/**7b** with 7:93 er of **6b** (entry 10). In an attempt to improve the chemoselectivity, only 1 equiv of H₂O₂ was used, however this resulted in reduced conversion with no perturbation to the product ratio (entry 11). Combining the beneficial structural features of **P4** and **P5**, **P6** features both the *N*-tosyl protecting group and α -Me(Pro) residue. Yet, this hybrid catalyst resulted in diminished conversion and chemoselectivity relative to **P5** (entry 12), thus **P5** was used as our lead catalyst to examine the scope and generality of this interesting transformation (Scheme 2).

Using **P5** under our optimized reaction conditions, oxidation of loratadine (**1a**) resulted in 74% conversion and 2.1:1 chemoselectivity with modest enantioselectivity of **6a** (64:35 er). Modulating the electronic nature of the phenyl urea moiety, both electron donating (**1c**) and withdrawing (**1d–i**) substituents were well tolerated in the reaction, affording *N*-oxides in up to 96:4 er. Interestingly, the more electron-withdrawing the substituent on the arene, the higher the conversion and enantioselectivity achieved, yet with diminished chemoselectivity. Substrates **1f–h** resulted in full consumption of the starting material, however, bis-oxidized compound **4** (containing both

an *N*-oxide and epoxide) was also detected in minor quantities (<15%).



Scheme 2. Substrate scope. All reactions were conducted in duplicate on a 0.05 mmol scale. Conversion (consumption of **1**) and ratios of **6**/**7** were determined using ¹H NMR (CDCl₃). Isolated yields of products are reported. Absolute configuration of *N*-oxides was determined by analogy to the single-crystal X-ray diffraction of **6e**.⁹ Crystal structure of **8h** shown at bottom with solvent molecules removed for clarity. [a] Bis-oxidized material was detected in <15% by ¹H NMR. [b] **8h** was isolated when reaction was conducted on a 0.2 mmol scale. [c] **7i** was not observed.

Notably, 3,5-bistrifluoromethylphenylurea substrate **1h** afforded *N*-oxide **6h** in >99:1 er, but modestly overturned the inherent chemoselectivity, slightly favoring the epoxide **7h** (63:37 er) in a 1:1.1 ratio of **6h**/**7h**. Using **P4**, 69:31 er was achieved for **7h** (see Supporting Information). Although not the goal of the present study, this result is interesting in that it represents the first example of an asymmetric preparation of a tetrasubstituted loratadine epoxide derivative with appreciable enantioselectivity.¹⁵ When performing the reaction with **1h** on a 0.2 mmol scale, we were able to isolate **8h** in 13% yield. This material was then used to obtain a crystal structure, showing the addition of both oxygen atoms to the same face of the molecule (Scheme 2, bottom). This may indicate that the substrate interacts with the peptide specifically to direct the delivery of oxygen atoms preferentially to one face of the molecule.

Of all the substrates tested in this reaction, pentafluorophenylurea analog **1i** was one of the most unique. While the enantioselectivity achieved (94:6 er) with **1i** was comparable to phenyl urea substrate **1b** (93:7 er), **1i** also exhibits complete chemoselectivity for *N*-oxidation, affording **6i** as the sole oxidation product in 44% yield.

We then examined analogs that deviated from the *N*-phenylurea motif. When replacing phenyl with *tert*-butyl (**1j**), the reaction proceeded with 74% conversion to a 1.1:1 ratio of **6j**/**7j** with moderate enantioselectivity (82:18 er). Replacing the urea with either a carbamate (**1a**, **1k**) or amide (**1l**–**1m**) resulted in lower enantioselectivity, but higher chemoselectivity. For example, **6k** was formed in a 2.3:1 ratio with 65:35 er, whereas the amide substrate **1l** produced a 1.8:1 ratio favoring **6l** in 71:29 er. We were curious about the performance of **1m**, as this analog resembles lonafarnib (**3**). However, **1m** was comparable to **1l**, giving a 2.0:1 ratio of **6m**/**7m** with 74:26 er of **6m**.

Mechanistic Studies. When comparing **2b** (urea), **2k** (carbamate), and **2l** (amide), we noted that as enantioselectivity increases for these substrates, chemoselectivity decreases. To better understand the role of the distal, putative directing substituent (green sphere, Scheme 2), we focused on substrates **1b**–**g**, which modulate the electronic nature of the *N*-phenylurea. **P2** was selected for this study since no bis-oxidized product (**8**) was detected when using this catalyst. The production of **8** may stem from a secondary kinetic resolution of **6** in which the minor enantiomer is preferentially funneled to **8**, thus artificially enhancing enantioselectivity of **6** and skewing the interpretation of any correlation. Plotting the enantioselectivity ($\Delta\Delta G^\ddagger$) of **6b**–**g** versus the corresponding Hammett σ_{para} values,¹⁶ a clear linear correlation ($\rho = +0.59$, $R^2 = 0.997$; Figure 2) was observed. As the *p*-substituent becomes more electron-withdrawing, the enantioselectivity increases. It is possible that the peptide backbone of the catalyst engages in a H-bond with the urea *N*–*H* of the substrate, positioning the activated aspartic peracid to deliver the oxygen atom to the pyridine with high levels of enantioinduction. This same binding interaction may also lead to increased epoxide formation (and also promotes the formation of the bis-oxidized product **8**), as the olefin and pyridine are in close spatial proximity (*vide infra*). Although the urea is

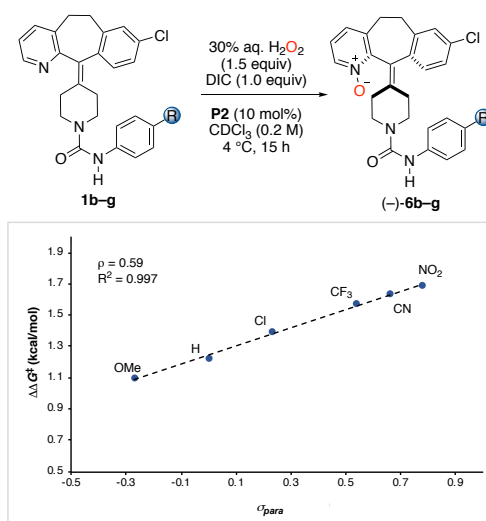


Figure 2. Hammett plot of enantioselectivity of **6b**–**g** ($\Delta\Delta G^\ddagger$) vs. σ_{para} .

quite removed from the site of oxidation, the conformation of the substrate presumably facilitates this interaction with the catalyst leading to high enantioselectivity. Consistent with this notion, enantioselectivity decreases significantly with substrates that lack the urea motif (**1a**, **1k**–**1m**, Scheme 2).

Conformational Dynamics. To gain more insight into the influencing structural features on our observed enantioselectivity, we then turned our attention to the structural dynamics of the *N*-oxidized products (**6**). As noted previously, loratadine in its ground state is chiral but not configurationally stable. Three main types of conformational mobility are easy to identify within the molecule: (a) ring-flipping of the cycloheptane, (b) chair-flipping of the piperidine ring, and (c) helix interconversion as substituents pass above and below the alkene (Figure 3a). This third motion is akin to the structural dynamics of overcrowded alkene-based molecular motors developed by Feringa and co-workers.¹⁷ Aspects of the flexibility of loratadine derivatives were identified in the late 1990s,^{8a-c} but barriers for all types of conformational interconversion or enantiomerization of helically chiral analogs, such as **4** and **5** (Figure 1b), were not reported in these early studies. Moreover, in reports of compounds **4** and (+)-**5**, Morgan *et al.* recognized that conformational enantiomers exist, but did not delineate the complex conformational landscape associated with the stereoisomerism.^{8c} Accordingly, we sought to understand and characterize (a) the modes of the conformational dynamics exhibited by these helically chiral compounds, (b) possible pathways for enantiomerization, and (c) their respective stereochemical stabilities.

Informing our study, the crystal structure of **6e** exhibits four conformers of the major *N*-oxide enantiomer, variably occupied in the crystallographic model (Figure 3a).⁹ DFT calculations were performed to determine the relative energies of each conformer and the barriers for interconversion (Figure 3b). Ground state optimization was performed on the four conformers observed crystallographically using truncated *N*-oxide (–)

9 for computational ease. Conformations **9a** and **9d** were slightly lower in energy than **9b** and **9c** likely due to the preferred equatorial orientation of the *N*-methylpiperidine. The barrier for piperidine ring-flipping was calculated to be 8.6 kcal/mol on average, depending on the cycloheptane conformation (Figure 3b). Cycloheptane ring-flipping was even more facile, with a barrier of 2.3 kcal/mol. Therefore, all four conformers should be easily accessible at room temperature for analogs of **1** and **6**, indicating that cycloheptane and piperidine ring flipping are not solely responsible for the observed, independently isolable and stable enantiomers.

In contrast, the barrier to enantiomerization was found to be significantly higher (be $\Delta G^\ddagger_{100^\circ\text{C}} = 28.5$ kcal/mol) as determined *via* high temperature (100 °C) racemization studies of **6h** (Figure 3c; see Supporting Information for details). This measurement supports that these helically chiral compounds are indeed stable at ambient temperatures for prolonged periods. Moreover, to test enantiomeric stability under more biologically relevant conditions, **6h** was heated at physiological

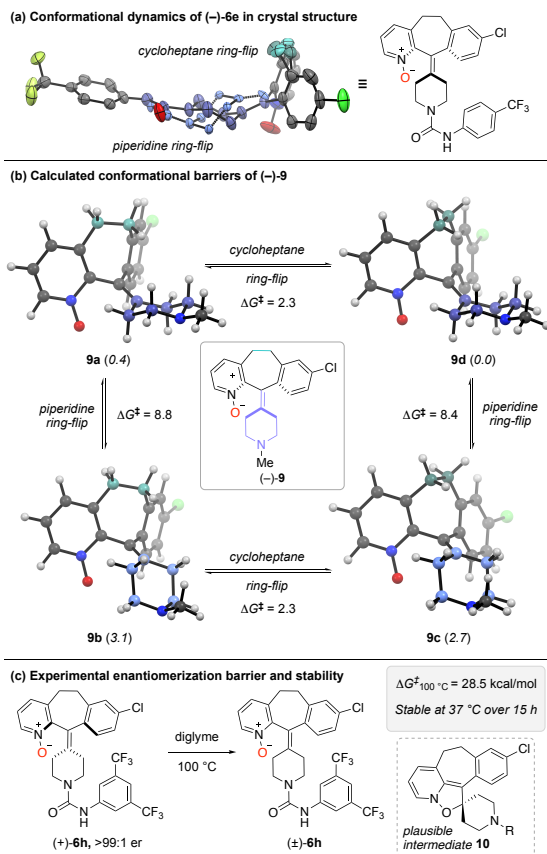


Figure 3. (a) Crystal structure of **6e**⁹ depicting conformational mobility of the cycloheptane (teal) and piperidine rings (purple). Hydrogens are omitted for clarity. (b) Computed ground state conformations and barriers to conformerization of (-)-**9a** calculated at the B3LYP/6-311++G(2d,3p) level. Energy values are reported in kcal/mol with ground state energies indicated in parenthesis. (c) Experimental barrier to enantiomerization at 100 °C and enantiomeric stability at 37 °C.

temperature (37 °C) for 15 h without detectable changes in enantioselectivity.

Although barriers for enantiomerization of related helically chiral compounds **4** and **5** were not determined, Morgan *et al.* report that heating (-)-**4** at 210 °C in diglyme also resulted in racemization, in analogy to our findings.^{8c} Thus, incorporation of a substituent β to the olefin, either through *N*-oxidation or bromination, leads to stable, helically chiral compounds, presumably due to the hindrance associated with the helix-interconverting *peri*-interaction¹⁸ engendered as the *N*-*O* bond passes the alkene substituents. However, that is also possible that alternative mechanisms for racemization of **6** operate, including a pathway involving the intermediacy of **10**, the product of a formal electrocyclic ring closure (Figure 3b).¹⁹ Yet, such a pathway would be less plausible for aryl bromides **4** and **5**. Nevertheless, we note that there is the potential for multiple mechanisms to operative, especially given that some decomposition of **6h** was observed during the prolonged heating required to determine the experimental enantiomerization barrier.

Antihistamine Activity. We then sought to assess how rigidifying the structure of loratadine through *N*-oxidation would affect its biological activity. Loratadine (**1a**) and desloratadine (**2**) are excellent functional antagonists of the human histamine H₁ receptor (H₁R),^{1,6,20} a member of the G-protein-coupled-receptor (GPCR) family. Therefore, we selected this as our biological target. We elected to use **1h** and **6h** as representatives of our substrate scope, as this peptide-catalyzed method provided direct access to enantiopure material (>99:1 er) of (+)-**6h**. Using **P4** under otherwise identical reaction conditions, (-)-**6h** was obtained in 98:2 er (see Supporting Information). HeLa cells were incubated with samples of conformationally labile compounds—loratadine (**1a**), **1h**, and desloratadine (**2**)—as well as each enantiomer of the structurally rigidified *N*-oxides **6a** and **6h**. The antagonist activity of these loratadine analogs was monitored by a change in intracellular calcium. When histamine binds H₁R, intracellular calcium increases; however, in the presence of antagonists like loratadine, the calcium increase is suppressed. Changes in the intracellular calcium concentration were measured with a fluorometric imaging plate reader (FLIPR) by excitation of calcium-sensitive fluorescent dye.

The relative peak fluorescence is plotted against the concentration (nM) of each compound, and the average IC₅₀ (nM) values (see Supporting Information for details) are shown in Figure 4. It is known that desloratadine (**2**; Figure 4, entry 1) is a more potent antagonist than loratadine (entry 2);⁶ however, we were unsure how a change from a carbamate to urea tail would affect activity. We were pleased to find that **1h** provided comparable antagonist activity to loratadine (**1a**; entries 2 *vs.* 3). With respect to loratadine *N*-oxidize (**6a**), both enantiomers were relatively inactive in our study, yet (-)-**6a** showed greater activity than (+)-**6a** (entries 4 *vs.* 5). This contrast was exaggerated with **6h**, as (-)-**6h** showed significant antagonist activity compared to (+)-**6h** (entries 4–7). Since the impact of rigidification is unique to each isomeric series, it is certainly

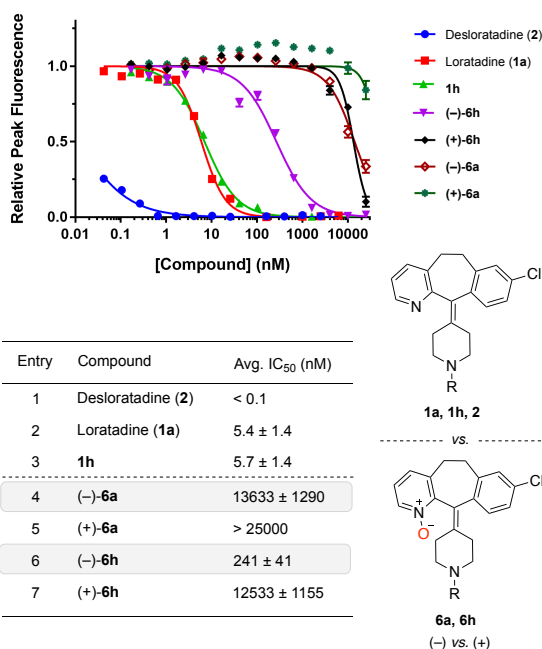


Figure 4. Peak fluorescence representing intracellular calcium concentration vs. concentration of loratadine analogs (top) and average IC₅₀ values of each analog (bottom).

possible that conformational dynamics contribute differentially as the independent stereoisomers interact with the target. That said, while it is not definitively known why **6h** performs better than **6a** in this assay, the conformation of these *N*-oxides unambiguously affects the antihistamine activity, with a preference to bind the orientation adopted by the (-)-enantiomer.

Docking Studies. Although a crystal structure depicting the binding orientation of loratadine or desloratadine with H₁R has not been obtained, Shimamura *et al.* were able to show the crystal structure of H₁R complexed with doxepin, a first-generation antagonist.²¹ Docking studies with H₁R and antagonists, including loratadine and desloratadine, have been performed.²² Using these conformationally flexible ligands, the preferred binding models depict loratadine in an orientation analogous to (-)-**6a**. To better understand the differential activity of our new compounds, we performed docking studies with (+)- and (-)-**6a** and **6h** with H₁R. The four major conformations (analogous to **9a-d** in Figure 3) of each enantiomer of **6a** and **6h** were constructed and then prepared with LigPrep.²³ Using Glide SP²⁴ with ring sampling disabled to maintain the initial conformations, the ligands were docked with H₁R in place of doxepin in the mainly hydrophobic binding pocket (see Supporting Information for details). The optimal scoring pose for each enantiomer of **6a** and **6h** is shown in Figure 5, which highlights several H-bonds between the ligands and protein.

Among the docking poses, the orientation of the ligand's carbonyl exhibited the greatest degree of variability, with the most flexibility exhibited by **6a**, likely due to its smaller tail. In some instances, such as with the top pose of (-)-**6a**, this carbonyl projects toward Lys-179, likely forming a H-bond with the ammonium of this residue. Contact with this residue has

been shown to be important for the selectivity of second-generation antihistamines.^{21,22} Alternatively, in the top docking poses with (+)-**6a** and (-)-**6h**, the carbonyl orients in the opposite direction towards Tyr-458.

There are several other differences between the docking poses of **6a** and **6h** with H₁R. Since the piperidine sp²-nitrogen is neutral at physiological pH, only **6h**, containing a urea moiety, is capable of H-bonding with the carboxylate of Asp-107. Interactions with Asp-107 has been reported to be essential for binding with H₁R.^{21,25} Moreover, in contrast to **6a**, the aryl urea moiety in **6h** enables this ligand to extend further into the hydrophobic binding pocket. A cation- π interaction is possible between the aryl-tail of **6h** and Lys-179, another key residue for antihistamine selectivity with H₁R.^{21,22} The increased network of noncovalent interactions between **6h** and H₁R may rationalize not only the difference in Glide SP score of each ligand (\sim 0.5 to \sim 1.1 kcal/mol; Figure 5) favoring **6h**, but also the enhanced antihistamine activity observed for **6h** as compared to **6a**.

Although our docking studies indicate that both (+)- and (-)-configurations of **6a** and **6h** can fit in this binding pocket, there are notable differences between the manner in which each enantiomer interacts with the surrounding residues. For example, a H-bond between the oxygen of the pyridine *N*-oxide and the hydroxyl group of Tyr-431 is only possible when the ligand is in the (-)-configuration. In the (+)-configuration, a possibly weaker halogen bond between the chlorine of the ligand and the carbonyl oxygen of Lys-191 is observed. Additionally, **6a** and **6h** are further stabilized in this binding pocket by several hydrophobic interactions, as has been seen in docking studies with loratadine as well.²² Both ligands can engage in T-shaped π - π interactions with Trp-428, a highly conserved key residue in GPCR activation, and Phe-432.²⁰ For the (-)-enantiomer, these interaction are with the aryl chloride ring of the ligand; in the (+)-configuration, the pyridine *N*-oxide ring participates in this NCI. The stereoelectronic differences between the aryl groups of the ligand impacts the strength of these π - π interactions, and, in turn, influences which enantiomer of **6a** and **6h** preferentially binds with H₁R. It is important to note that the Glide SP scores of each enantiomer are not markedly different (\sim 0.1 to \sim 0.5 kcal/mol; Figure 5); however, these docking poses provide a tool to speculate about the observed enantiomer-dependent antihistamine activity, which are more pronounced in the experimental assays (Figure 4).

Conclusion

In conclusion, we have developed a strategy to chemo- and enantioselectively synthesize analogs of loratadine *N*-oxide using Asp-containing peptide catalysts. With our best cases, loratadine *N*-oxide analog **6h** was produced in >99:1 er, and **1i** demonstrated complete chemoselectivity for *N*-oxidize **6i**. These helically chiral products are configurationally stable under physiological conditions, with a barrier of enantiomerization of $\Delta G^\ddagger_{100^\circ\text{C}} = 28.5$ kcal/mol. Loratadine analogs with a urea

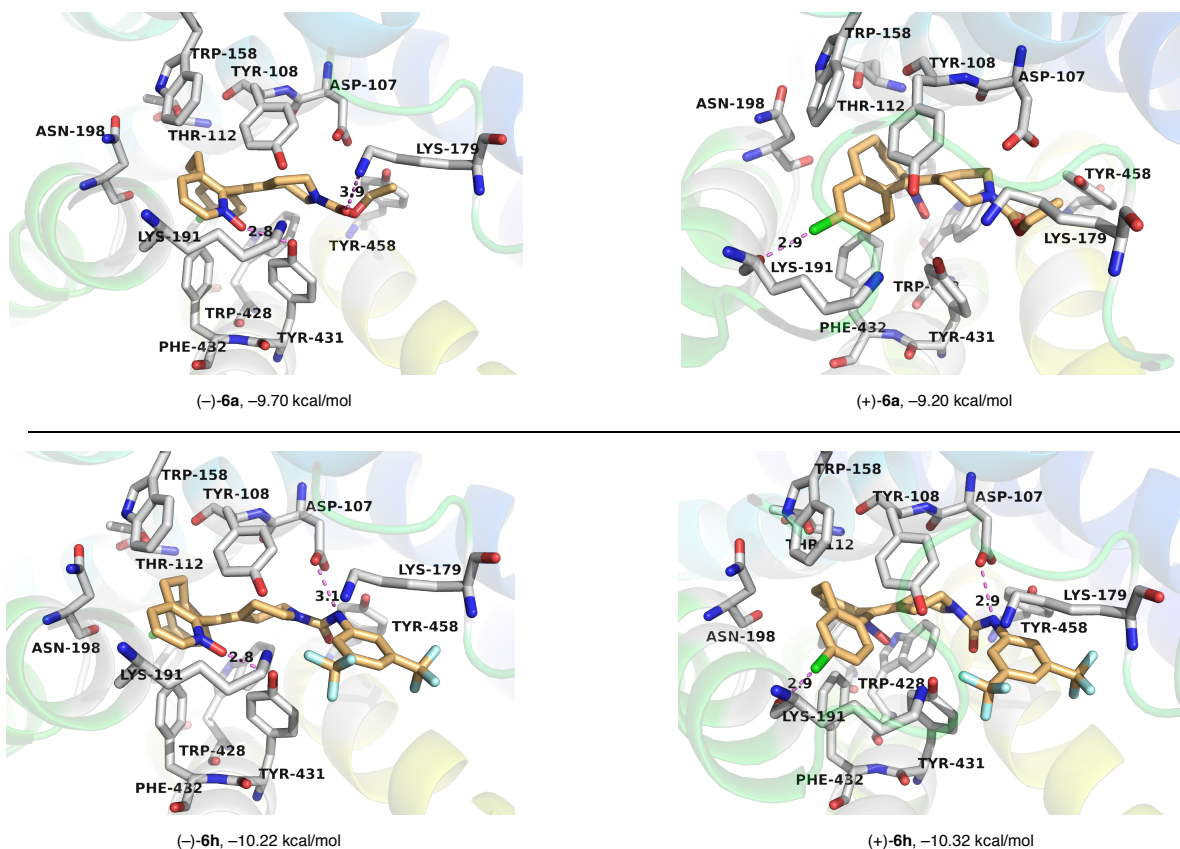


Figure 5. Top scoring docking binding poses of **6a** (top) and **6h** (bottom) with H₁R. Glide SP scores depicted below poses. Key intermolecular H-bonds are shown in violet with distances (Å) between heavy atoms; other NCIs are not highlighted for clarity. H-atoms are also omitted for clarity.

moiety displayed equivalent antihistamine activity to carbamate-bearing loratadine, which was supported by our docking studies. Moreover, we have illuminated the role of conformational dynamics on the biological activity of loratadine and desloratadine. Given the preference for H₁R to interact with the (-)-enantiomer of the loratadine *N*-oxide analogs, it is quite possible that flexible loratadine (**1a**) and desloratadine (**2**) adopt a conformation akin to (-)-**6** when bound to this target, as supported by docking studies. We hope that these enantio-enriched loratadine *N*-oxide products may be valuable for identifying new or improved active pharmaceutical ingredients, or as tools to study the binding of loratadine and related analogs to their various biological targets.

ASSOCIATED CONTENT

Supporting Information

The Supporting Information is available free of charge on the ACS Publications website.

Experimental details and characterization information for peptides, loratadine analogs, and oxidized products; experimental and calculated data for barriers of enantiomerization and conformerization; antihistamine activity testing details; crystallographic data

for (±)-**6b** (1983136), (-)-**6f** (1983464), and **8h** (1983156); and computational docking information (PDF)

Primary NMR Data files, HPLC traces, IR spectra, and HRMS for peptides, loratadine analogs, and oxidized products (.zip)

AUTHOR INFORMATION

Corresponding Author

*Email for S.J.M: scott.miller@yale.edu

Funding Sources

This research was supported by the National Institutes of Health (NIHGMS R35 132092) and the National Science Foundation Graduate Research Fellowship (DGE-112249).

ACKNOWLEDGMENT

The authors would like to thank Dr. James Herrington and the Yale Center for Molecular Discovery for performing the biological activity assays. We also acknowledge Dr. Brandon Mercado for X-ray crystallographic support and expertise. The authors are grateful to Prof. William L. Jorgensen, Dr. Julian Tirado-Rives, and Dr. Ana S.

Newton for helpful discussions and assistance with the docking studies. For insightful conversations and access to the Asp-peptide library, we would like to thank Dr. Sheng-Ying Hsieh, Dr. Yu Tang and Dr. Simone Crotti. For critical suggestions and assistance with manuscript preparations, we thank Dr. Margaret Hilton, Dr. Hyung Yoon, and Gavin Coombs.

ABBREVIATIONS

(α -Me)Pro: α -methyl-L-proline; Acpc: 1-aminocyclopropane carboxylic acid; Boc: *tert*-butoxycarbonyl; DIC: *N,N'*-diisopropylcarbodiimide; DKR: dynamic kinetic resolution; FLIPR: fluorescence image plate reader; GPCR: G-protein-coupled-receptor; H-bond: hydrogen bond; H₁R: human histamine H₁ receptor; KR: kinetic resolution; *m*-CPBA: *meta*-chloro-peroxybenzoic acid; Ts: tosyl

REFERENCES

- Hilbert, J.; Radwanski, E.; Weglein, R.; Luc, V.; Perentesis, G.; Symchowicz, S.; Zampaglione, N. Pharmacokinetics and Dose Proportionality of Loratadine. *J. Clin. Pharmacol.* **1987**, *27*, 694–698.
- (a) Njoroge, F. G.; Taveras, A. G.; Kelly, J.; Remiszewski, S.; Mallams, A. K.; Wolin, R.; Afonso, A.; Cooper, A. B.; Rane, D. F.; Liu, Y.-T.; Wong, J.; Vibulbhan, B.; Pinto, P.; Deskus, J.; Alvarez, C. S.; del Rosario, J.; Connolly, M.; Wang, J.; Desai, J.; Rossmann, R. R.; Bishop, W. R.; Patton, R.; Wang, L.; Kirschmeier, P.; Bryant, M. S.; Nomeir, A. A.; Lin, C. C.; Liu, M.; McPhail, A. T.; Doll, R. J.; Girijavallabhan, V. M.; Ganguly, A. K. (+)-4-[2-[4-(8-Chloro-3,10-dibromo-6,11-dihydro-5H-benzo[5,6]cyclohepta [1,2-b]-pyridin-11(R)-yl]-1-piperidinyl]-2-oxo-ethyl]-1-piperidin-ecarboxamide (SCH-66336): A Very Potent Farnesyl Protein Transferase Inhibitor as a Novel Antitumor Agent. *J. Med. Chem.* **1998**, *41*, 4890–4902; (b) Soule, B. P.; Simone, N. L.; DeGraff, W. G.; Choudhuri, R.; Cook, J. A.; Mitchell, J. B. Loratadine dysregulates cell cycle progression and enhances the effect of radiation in human tumor cell lines. *Radiat. Oncol.* **2010**, *5*, 8; (c) Gatne, P. S.; Viswanathan, C. L.; Ambre, P. K.; Juvekar, A. Design, Synthesis and Evaluation of Novel 1-(Substituted Acetyl)-4-(10-Bromo-8-Chloro-5,6-Dihydro-11H-Benzo[5,6]Cyclohepta [1,2-B]Pyridine-11-Ylidene)-piperidines as Antitumor Agents and Farnesyl Protein Transferase Inhibitors. *Indian J Pharm Sci* **2010**, *72*, 663–667; (d) Ellegaard, A.-M.; Dehlendorff, C.; Vind, A. C.; Anand, A.; Cederkvist, L.; Petersen, N. H. T.; Nylandsted, J.; Stenvang, J.; Mellemegaard, A.; Østerlind, K.; Friis, S.; Jäättelä, M. Repurposing Cationic Amphiphilic Antihistamines for Cancer Treatment. *EBioMedicine* **2016**, *9*, 130–139; (e) Chen, T.; Hu, Y.; Liu, B.; Huang, X.; Li, Q.; Gao, N.; Jin, Z.; Jia, T.; Guo, D.; Jin, G. Combining thioridazine and loratadine for the treatment of gastrointestinal tumor. *Oncol. Lett.* **2017**, *14*, 4573–4580; (f) Olsson, H. L.; Broberg, P.; Einefors, R.; Fritz, I. Effects of antihistamine use on survival in breast cancer. *J. Clin. Oncol.* **2018**, *36*, e12527–e12527; (g) Desai, P.; Thakkar, A.; Ann, D.; Wang, J.; Prabhu, S. Loratadine self-microemulsifying drug delivery systems (SMEDDS) in combination with sulforaphane for the synergistic chemoprevention of pancreatic cancer. *Drug Deliv. Transl. Res.* **2019**, *9*, 641–651.
- Moon, H.-R.; Jo, S. Y.; Kim, H. T.; Lee, W. J.; Won, C. H.; Lee, M. W.; Choi, J. H.; Chang, S. E. Loratadine, an H₁(1) Antihistamine, Inhibits Melanogenesis in Human Melanocytes. *Biomed. Res. Int.* **2019**, *2019*, 5971546–5971546.
- Cutrona, N.; Gillard, K.; Ulrich, R.; Seemann, M.; Miller, H. B.; Blackledge, M. S. From Antihistamine to Anti-infective: Loratadine Inhibition of Regulatory PASTA Kinases in Staphylococci Reduces Biofilm Formation and Potentiates β -Lactam Antibiotics and Vancomycin in Resistant Strains of Staphylococcus aureus. *ACS Infect. Dis.* **2019**, *5*, 1397–1410.
- Cuboni, S.; Devigny, C.; Hoogeland, B.; Strasser, A.; Pomplun, S.; Hauger, B.; Höfner, G.; Wanner, K. T.; Eder, M.; Buschauer, A.; Holsboer, F.; Hausch, F. Loratadine and Analogues: Discovery and Preliminary Structure–Activity Relationship of Inhibitors of the Amino Acid Transporter B0AT2. *J. Med. Chem.* **2014**, *57*, 9473–9479.
- (a) Anthes, J. C.; Gilchrist, H.; Richard, C.; Eckel, S.; Hesk, D.; West, R. E.; Williams, S. M.; Greenfeder, S.; Billah, M.; Kreutner, W.; Egan, R. W. Biochemical characterization of desloratadine, a potent antagonist of the human histamine H₁ receptor. *Eur. J. Pharmacol.* **2002**, *449*, 229–237; (b) Canonica, G. W.; Blaiss, M. Antihistaminic, anti-inflammatory, and antiallergic properties of the non-sedating second-generation antihistamine desloratadine: a review of the evidence. *World Allergy Organ. J.* **2011**, *4*, 47–53.
- (a) Clayden, J.; Moran, W. J.; Edwards, P. J.; LaPlante, S. R. The Challenge of Atropisomerism in Drug Discovery. *Angew. Chem. Int. Ed.* **2009**, *48*, 6398–6401; (b) LaPlante, S. R.; Fader, L. D.; Fandrick, K. R.; Fandrick, D. R.; Hucke, O.; Kemper, R.; Miller, S. P. F.; Edwards, P. J. Assessing Atropisomer Axial Chirality in Drug Discovery and Development. *J. Med. Chem.* **2011**, *54*, 7005–7022; (c) Kumarasamy, E.; Raghunathan, R.; Sibi, M. P.; Sivaguru, J. Nonbiaryl and Heterobiaryl Atropisomers: Molecular Templates with Promise for Atropselective Chemical Transformations. *Chem. Rev.* **2015**, *115*, 11239–11300; (d) Smyth, J. E.; Butler, N. M.; Keller, P. A. A twist of nature - the significance of atropisomers in biological systems. *Nat. Prod. Rep.* **2015**, *32*, 1562–1583; (e) Glunz, P. W. Recent encounters with atropisomerism in drug discovery. *Bioorganic Med. Chem. Lett.* **2018**, *28*, 53–60; (f) Toenjes, S. T.; Gustafson, J. L. Atropisomerism in medicinal chemistry: challenges and opportunities. *Future Med. Chem.* **2018**, *10*, 409–422; (g) Wang, Y.-B.; Tan, B. Construction of Axially Chiral Compounds via Asymmetric Organocatalysis. *Acc. Chem. Res.* **2018**, *51*, 534–547; (h) Mancinelli, M.; Bencivenni, G.; Pecorari, D.; Mazzanti, A. Stereochemistry and Recent Applications of Axially Chiral Organic Molecules. *Eur. J. Org. Chem.*, **2020**, DOI: [10.1002/ejoc.201901918](https://doi.org/10.1002/ejoc.201901918).
- (a) Piwinski, J. J.; Wong, J. K.; Chan, T. M.; Green, M. J.; Ganguly, A. K. Hydroxylated metabolites of loratadine: an example of conformational diastereomers due to atropisomerism. *J. Org. Chem.* **1990**, *55*, 3341–3350; (b) Kaminski, J. J.; Carruthers, N. I.; Wong, S.-C.; Chan, T.-M.; Motassim Billah, M.; Tozzi, S.; McPhail, A. T. Conformational considerations in the design of dual antagonists of platelet-activating factor (PAF) and histamine. *Bioorganic Med. Chem.* **1999**, *7*, 1413–1423; (c) Morgan, B.; Zaks, A.; Dodds, D. R.; Liu, J.; Jain, R.; Megati, S.; Njoroge, F. G.; Girijavallabhan, V. M. Enzymatic Kinetic Resolution of Piperidine Atropisomers: Synthesis of a Key Intermediate of the Farnesyl Protein Transferase Inhibitor, SCH66336. *J. Org. Chem.* **2000**, *65*, 5451–5459; (d) Woollam, G. R.; Neumann, M. A.; Wagner, T.; Davey, R. J. The importance of configurational disorder in crystal structure prediction: the case of loratadine. *Faraday Discuss.* **2018**, *211*, 209–234.
- Hsieh, S.-Y.; Tang, Y. U.; Crotti, S.; Stone, E. A.; Miller, S. J. Catalytic Enantioselective Pyridine *N*-Oxidation. *J. Am. Chem. Soc.* **2019**, *141*, 18624–18629.
- (a) Ramanathan, R.; Alvarez, N.; Su, A. D.; Chowdhury, S.; Alton, K.; Stauber, K.; Patrick, J. Metabolism and excretion of loratadine in male and female mice, rats and monkeys. *Xenobiotica* **2005**, *35*, 155–189; (b) Chen, G.; Daaro, I.; Pramanik, B. N.; Piwinski, J. J. Structural characterization of in vitro rat liver microsomal metabolites of antihistamine desloratadine using LTQ-Orbitrap hybrid mass spectrometer in combination with online hydrogen/deuterium exchange HR-LC/MS. *J. Mass Spectrom.* **2009**, *44*, 203–213; (c) Habicht, S. C.; Duan, P.; Vinueza, N. R.; Fu, M.;

Kenttämä, H. I. Liquid chromatography/tandem mass spectrometry utilizing ion-molecule reactions and collision-activated dissociation for the identification of N-oxide drug metabolites. *J. Pharmaceut. Biomed.* **2010**, *51*, 805–811.

11. (a) Cerrada, V.; Matía-Martín, M. P.; Novella, J. L.; Alvarez-Builla, J. Synthesis of 2- and 4-hydroxymethyl Loratadine, usual impurities in Loratadine syrup formulations. *ARKIVOC* **2005**, *2005*, 200–206; (b) Singh, P.; Dhakarey, R. K. S. Synthesis of 2- and 4-Carboxylic Acid Derivatives of Loratadine and Desloratadine. *Rasayan J. Chem.* **2009**, *2*, 436–440.

12. Alford, J. S.; Abascal, N. C.; Shugrue, C. R.; Colvin, S. M.; Romney, D. K.; Miller, S. J. Aspartyl Oxidation Catalysts That Dial In Functional Group Selectivity, along with Regio- and Stereoselectivity. *ACS Cent. Sci.* **2016**, *2*, 733–739.

13. (a) Haque, T. S.; Little, J. C.; Gellman, S. H. Stereochemical Requirements for β -Hairpin Formation: Model Studies with Four-Residue Peptides and Depsipeptides. *J. Am. Chem. Soc.* **1996**, *118*, 6975–6985; (b) Metrano, A. J.; Abascal, N. C.; Mercado, B. Q.; Paulson, E. K.; Hurlley, A. E.; Miller, S. J. Diversity of Secondary Structure in Catalytic Peptides with β -Turn-Biased Sequences. *J. Am. Chem. Soc.* **2017**, *139*, 492–516.

14. (a) Taylor, M. S.; Jacobsen, E. N. Asymmetric Catalysis by Chiral Hydrogen-Bond Donors. *Angew. Chem. Int. Ed.* **2006**, *45*, 1520–1543; (b) Doyle, A. G.; Jacobsen, E. N. Small-Molecule H-Bond Donors in Asymmetric Catalysis. *Chem. Rev.* **2007**, *107*, 5713–5743; (c) MacMillan, D. W. C. The advent and development of organocatalysis. *Nature* **2008**, *455*, 304–308; (d) Knowles, R. R.; Jacobsen, E. N. Attractive noncovalent interactions in asymmetric catalysis: Links between enzymes and small molecule catalysts. *Proc. Natl. Acad. Sci. U.S.A.* **2010**, *107*, 20678–20685; (e) Toste, F. D.; Sigman, M. S.; Miller, S. J. Pursuit of Noncovalent Interactions for Strategic Site-Selective Catalysis. *Acc. Chem. Res.* **2017**, *50*, 609–615; (f) Sawano, T.; Yamamoto, H. Substrate-Directed Catalytic Selective Chemical Reactions. *J. Org. Chem.* **2018**, *83*, 4889–4904; (g) Metrano, A. J.; Miller, S. J. Peptide-Based Catalysts Reach the Outer Sphere through Remote Desymmetrization and Atroposelectivity. *Acc. Chem. Res.* **2019**, *52*, 199–215.

15. (a) Brandes, B. D.; Jacobsen, E. N. Enantioselective catalytic epoxidation of tetrasubstituted olefins. *Tetrahedron Lett.* **1995**, *36*, 5123–5126; (b) Katsuki, T.; V., M., Asymmetric Epoxidation of Allylic Alcohols: the Katsuki–Sharpless Epoxidation Reaction. *Organic Reactions*, **2004**, 1–299; (c) Irie, R.; Uchida, T.; Matsumoto, K. Katsuki Catalysts for Asymmetric Oxidation: Design Concepts, Serendipities for Breakthroughs, and Applications. *Chem. Lett.* **2015**, *44*, 1268–1283.

16. Hansch, C.; Leo, A.; Taft, R. W. A survey of Hammett substituent constants and resonance and field parameters. *Chem. Rev.* **1991**, *91*, 165–195.

17. (a) Cnossen, A.; Kistemaker, J. C. M.; Kojima, T.; Feringa, B. L. Structural Dynamics of Overcrowded Alkene-Based Molecular Motors during Thermal Isomerization. *J. Org. Chem.* **2014**, *79*, 927–935; (b) Kassem, S.; van Leeuwen, T.; Lubbe, A. S.; Wilson, M. R.; Feringa, B. L.; Leigh, D. A. Artificial molecular motors. *Chem. Soc. Rev.* **2017**, *46*, 2592–2621.

18. Balasubramanian, V. *peri*-Interaction in Naphthalene Derivatives. *Chem. Rev.* **1966**, *66*, 567–641.

19. (a) Riediker, M.; Graf, W. “Isolierte” olefinische Doppelbindungen als 2π -Komponente in [8+2]-Cycloadditionen. *Angew. Chemie.* **1981**, *93*, 491–493; (b) Biswas, A.; Karmakar, U.; Pal, A.; Samanta, R. Copper-Catalyzed Regioselective Cascade Alkylation and Cyclocondensation of Quinoline N-Oxides with Diazo Esters: Direct Access to Conjugated π -Systems. *Chem. Eur. J.* **2016**, *22*, 13826–13830.

20. Bakker, R. A.; Schoonus, S. B. J.; Smit, M. J.; Timmerman, H.; Leurs, R. Histamine H₁-Receptor Activation of Nuclear Factor- κ B: Roles for G $\beta\gamma$ - and G $\alpha_q/11$ -Subunits in Constitutive and Agonist-Mediated Signaling. *Mol. Pharmacol.* **2001**, *60*, 1133–1142.

21. Shimamura, T.; Shiroishi, M.; Weyand, S.; Tsujimoto, H.; Winter, G.; Katritch, V.; Abagyan, R.; Cherezov, V.; Liu, W.; Han, G. W.; Kobayashi, T.; Stevens, R. C.; Iwata, S. Structure of the human histamine H₁ receptor complex with doxepin. *Nature* **2011**, *475*, 65–70.

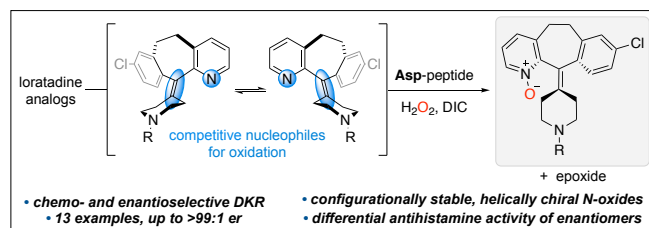
22. (a) Kiss, R.; Kovári, Z.; Keserű, G. M. Homology modelling and binding site mapping of the human histamine H₁ receptor. *Eur. J. Med. Chem.* **2004**, *39*, 959–967; (b) Jongejan, A.; Leurs, R. Delineation of Receptor-Ligand Interactions at the Human Histamine H₁ Receptor by a Combined Approach of Site-Directed Mutagenesis and Computational Techniques – or – How to Bind the H₁ Receptor. *Arch. Pharm.* **2005**, *338*, 248–259; (c) Riza, Y. M.; Parves, M. R.; Tithi, F. A.; Alam, S. Quantum chemical calculation and binding modes of H₁R; a combined study of molecular docking and DFT for suggesting therapeutically potent H₁R antagonist. *In Silico Pharmacol.* **2019**, *7*, 1.

23. Schrödinger Release 2015-4: LigPrep, Schrödinger, LLC, New York, NY, 2015.

24. (a) Friesner, R. A.; Banks, J. L.; Murphy, R. B.; Halgren, T. A.; Klicic, J. J.; Mainz, D. T.; Repasky, M. P.; Knoll, E. H.; Shelley, M.; Perry, J. K.; Shaw, D. E.; Francis, P.; Shenkin, P. S., Glide: A New Approach for Rapid, Accurate Docking and Scoring. 1. Method and Assessment of Docking Accuracy. *J. Med. Chem.* **2004**, *47*, 1739–1749; (b) Halgren, T. A.; Murphy, R. B.; Friesner, R. A.; Beard, H. S.; Frye, L. L.; Pollard, W. T.; Banks, J. L., Glide: A New Approach for Rapid, Accurate Docking and Scoring. 2. Enrichment Factors in Database Screening. *J. Med. Chem.* **2004**, *47*, 1750–1759.

25. (a) Ohta, K.; Hayashi, H.; Mizuguchi, H.; Kagamiyama, H.; Fujimoto, K.; Fukui, H. Site-Directed Mutagenesis of the Histamine H₁ Receptor: Roles of Aspartic Acid107, Asparagine198 and Threonine194. *Biochem. Biophys. Res. Commun.* **1994**, *203*, 1096–1101; (b) Nonaka, H.; Otaki, S.; Ohshima, E.; Kono, M.; Kase, H.; Ohta, K.; Fukui, H.; Ichimura, M. Unique binding pocket for KW-4679 in the histamine H₁ receptor. *Eur. J. Pharmacol.* **1998**, *345*, 111–117; (c) Bruysters, M.; Pertz, H. H.; Teunissen, A.; Bakker, R. A.; Gillard, M.; Chatelain, P.; Schunack, W.; Timmerman, H.; Leurs, R. Mutational analysis of the histamine H₁-receptor binding pocket of histaprodifens. *Eur. J. Pharmacol.* **2004**, *487*, 55–63.

Insert Table of Contents artwork here



1
2
3
4
5
6
7
8
9
10
11
12
13
14
15
16
17
18
19
20
21
22
23
24
25
26
27
28
29
30
31
32
33
34
35
36
37
38
39
40
41
42
43
44
45
46
47
48
49
50
51
52
53
54
55
56
57
58
59
60